

Document downloaded from:

<http://hdl.handle.net/10251/79518>

This paper must be cited as:

López, JJ.; Salvador Rubio, FJ.; De La Garza De Leon, O.; Arregle, JJP. (2012). Characterization of the pressure losses in a common rail diesel injector. Proceedings of the Institution of Mechanical Engineers, Part D: Journal of Automobile Engineering. 226(12):1697-1706. doi:10.1177/0954407012447020.



The final publication is available at

<http://dx.doi.org/10.1177/0954407012447020>

Copyright SAGE Publications (UK and US)

Additional Information

Title

Characterization of the pressure losses in a common rail diesel injector

Authors

(1) J. Javier López, F. Javier Salvador and Oscar A. de la Garza.

(2) Jean Arrègle.

Affiliation

(1) CMT-Motores Térmicos

(2) Departamento de Máquinas y Motores Térmicos

Universitat Politècnica de València, Spain

Camino de Vera, s/n. 46022 Valencia, SPAIN

Corresponding author

J. Javier López

CMT-Motores Térmicos

Universitat Politècnica de València

Camino de Vera, s/n. 46022 Valencia, SPAIN

e-mail: jolosan3@mot.upv.es

Tlf: +34 963 879 232, Fax: +34 963 877 659

Abstract

A methodology to characterise the pressure losses in quasi-steady conditions (i.e. at full needle lift) of common rail diesel injectors was developed. The aim was to quantify the error when experimental results of nozzle internal flow are compared with CFD results, where pressure losses are usually neglected. The proposed methodology is based mainly on experimental tests that are complemented with some approximate calculations, based on the physics of the phenomenon, to take into account the effect of the needle deformation. The results obtained in the work lead to two important conclusions: on the one hand, that it is dangerous to extrapolate results relative to the injection (internal flow, spray atomization, spray penetration:.) and combustion processes from low permeability nozzles (e.g. single-hole nozzles) to high permeability nozzles (e.g. multi-hole nozzles), and, on the other hand, that the comparison of these results between experiments and CFD simulations should be carried out carefully, because the pressure losses in the injector can be high under certain conditions. Finally, people working on the study of the injection and/or combustion processes, through experiments or simulations, will find here some interesting information to better know the actual injection pressure to be used in their analysis and/or simulations.

Keywords

Diesel injector, diesel nozzle, internal flow, pressure losses.

Notation

A	Cross-sectional area
C_d	Discharge coefficient

CFD	Computational Fluid Dynamics
D	Diameter of the inner part of the injector holder
D_A	Diameter of the cone of the needle seat
D_S	Diameter of the nozzle sac
f	Friction coefficient
h	Needle lift
K_{def_needle}	Deformation coefficient of the needle
L	Injector holder length
\dot{m}	Mass flow rate
M_1	Intermediate value to simplify Equation 16
M_2	Intermediate value to simplify Equation 17
P	Pressure
R^2	Coefficient of determination
t	Time
u	Velocity

Greek symbols

α	Angle of the needle tip
β_1	Characteristic angle to determine the cross-sectional area at the needle seat
ΔP	Pressure losses
ε	Rugosity
μ	Dynamic viscosity
ρ	Density
σ	Angle of the needle seat

Subscripts

<i>back</i>	In the enclosure where the fuel is injected
<i>f</i>	Referred to the fuel
<i>global</i>	Referred to all the injector (injector holder + needle seat)
<i>IH</i>	Injector holder
<i>new</i>	Recalculated value in an algorithm
<i>orif</i>	Referred to the nozzle orifice
<i>rail</i>	Referred to the common rail
<i>sac</i>	Referred to the nozzle sac
<i>seat</i>	Referred to the needle seat
<i>with_deformation</i>	Taking into account the needle deformation

1 Introduction

Pollutant emissions standards applicable to automobiles are more and more restrictive nowadays [1–3], encouraging engine manufacturers to design and build more efficient and environment-friendly engines. For this reason, different methods to lowering pollutant emissions are currently under investigation. One of the explored methods when dealing with diesel engines is the injector nozzle geometry [4–14].

The first step in order to study the effect of the nozzle geometry on the combustion process is the analysis of the flow at the nozzle orifice [15]. This flow is usually analysed taking into account the rail pressure, P_{rail} , as the upstream pressure, and the back pressure (i.e. the pressure at the enclosure where the nozzle discharges), P_{back} , as the downstream pressure. To be more strict, the real upstream pressure, i.e. the pressure at the nozzle sac, P_{sac} , should be used instead of P_{rail} . In fact, when the rail pressure is used any of the following two assumptions is implicitly taken: (1) the pressure losses along the injector are

small compared to the rail pressure, or (2) these pressure losses are proportional to the pressure drop at the nozzle orifice. An example to illustrate this way to proceed is when CFD calculations of the flow inside a diesel nozzle are performed, where P_{sac} is assumed to be P_{rail} , thus neglecting the pressure losses. But it is really dangerous to take any assumption when it is not validated, and to the authors knowledge nobody has validated any of the two assumptions mentioned above.

For this reason, the main objective of this work is to validate these two assumptions. For this purpose a methodology to determine pressures losses along the injector in quasi-steady conditions (i.e. at full needle lift) will be defined, to quantify afterwards the error introduced when these pressure losses are neglected.

This paper is divided in four more sections. In the second section, a brief description of the experimental arrangement used to quantify the pressure losses along the injector is presented. In the third section, the effect of the needle deformation on the pressure losses is analysed. In the fourth section, the pressure losses in a real nozzle will be quantified applying the knowledge gained in the two previous sections. Finally, in the last section the main conclusions of the study will be presented.

2 Determination of the injector pressure losses

In Figure 1, the layout of the experimental facility designed for the measurement of the injector pressure losses is shown. The injector (a second generation, solenoid injector used in a 4-cylinder, 1.6 litre HDI diesel engine) is mounted in the discharge chamber, which will be filled with diesel fuel as the injector is operated. The pressure in the chamber is regulated at the desired level by means of the back pressure regulation valve. The tip of the nozzle was removed (the part containing the orifices) so as to make the nozzle sac accessible. Now the sac pressure can be controlled (in fact, it is the discharge chamber pressure) and the injector pressure losses can be characterised. In an actual injector, operating at nominal conditions, no cavitation in the injector holder exists. In these

experiments, however, the sac pressure is now directly controlled, and attention has to be paid to avoid cavitation in the injector holder. For this reason a high pressure level in the discharge chamber ($P_{sac} = 5$ MPa) was used during the experiments, which was enough to avoid cavitation in any part of the injector holder.

The experiments were performed with a constant back pressure, and only P_{rail} was modified to change the operating conditions. For each operating point (i.e. a given P_{rail}), the mass flow rate going through the injector in steady conditions was measured. To achieve a continuous flow, the ball valve controlling the opening of the injector control volume was removed, so as to have the injector open continuously. (Any detail about the different parts of a common rail diesel injector can be found e.g. in [16]). The experimental results concerning pressure losses in the injector¹ are shown in Figure 2. In the Figure it can be observed that pressure losses in the injector can be quite high in some cases (at high mass flow rates). All the experimental points were fitted to the following equation:

$$\Delta P_{IH+seat}[MPa] = 0.0514 \cdot (\dot{m}_f[g/s])^{1.7761} \quad R^2 = 0.9954 \quad (1)$$

where the pressure losses include those of the injector holder (IH) and the needle seat. As the reader might guess, this equation is strictly only valid for the type of injector holder used in the present experiment. However, as the injector holder is representative of those currently used in automotive applications, the results of this paper can also be taken as representative of what might be expected in other injectors similar to the one investigated here. As the coefficient of determination, R^2 , of the fit is very near 1, this equation will be used to interpolate and/or slightly extrapolate pressure losses to any other value of the mass flow rate.

It is worthy to underline that even though the mass flow rate range tested is realistic²,

¹As it will be justified later, they were obtained in simplified conditions, with an unrealistic needle deformation.

²Higher values of mass flow rate were unable to be tested because of limitations in the injection pump: in fact, the mass flow rate in these tests was continuous, whereas the injection pump is designed to operate with relatively short injections (a few crank angle degrees every engine cycle).

pressures are not. In fact, P_{sac} (equal to P_{back} in this facility) was limited to 5 MPa because of the mechanical strength of the vessel, and consequently P_{rail} could not be much higher. In real operating conditions, even if the value of $P_{rail} - P_{sac}$ is similar to the one used in the experiments, the absolute values for P_{rail} and P_{sac} are much higher.

According to literature, P_{rail} has an effect on three aspects: on fuel properties [17], on injector internal leakage [18], and on needle deformation [19,20]. Concerning the first aspect, several authors [19,21] consider the fuel properties constant at different rail pressures, and therefore this effect should not be very important. Concerning the second aspect, some authors [16,19] assume that the sealing between the different injector parts is perfect, and so internal leakage can be considered insignificant. And concerning the third aspect, the elastic deformation of some elements (as for instance, the needle) can be very big, even near the same order of magnitude of their displacement, because of the high pressure [16,22]. If the needle is deformed, a change in the cross-sectional area between the needle surface and the needle seat takes place, which may affect the pressure losses. The analysis of this effect is presented and discussed in the next section.

3 Effect of the needle deformation on pressure losses

The effect of the needle deformation on the pressure losses cannot be studied experimentally in the facility presented in the previous section because of some physical limitations (the discharge pressure is limited to a maximum value of 5 MPa). For this reason the study of this effect will be addressed by an approximate calculation based on the physics of the phenomena involved. The details of this calculation will be presented in four steps. First, the effect of the rail pressure on the needle deformation is analysed. Second, the effect of the needle deformation on the pressure losses at the nozzle seat is studied. Third, the relationship between the mass flow rate and the pressure drop in the nozzle is characterised and, finally a calculation algorithm is defined so as to put all the aspects together. These steps are detailed in the following paragraphs.

3.1 Effect of the rail pressure on the needle deformation

The needle deformation affects the actual needle lift according to Equation 2:

$$h = h_o + K_{def_needle} \cdot P_{rail} \quad (2)$$

where h is the needle lift when the needle is deformed, h_o is the nominal needle lift, K_{def_needle} is the elasticity constant of the needle and P_{rail} is the rail pressure. In this equation it is assumed that P_{rail} is the main responsible for the needle deformation, because of two main reasons: firstly, because this pressure is the one that reaches the bottom part of the needle, as the pressure losses in the injector holder are negligible (this will be demonstrated afterwards), and, secondly, because the contact between the needle and its seat is nearly at the tip of the needle (see, e.g., Figure 3), and consequently the main part of the needle tip is mostly affected by P_{rail} , and not by P_{sac} .

In order to see the effect of P_{rail} on the needle deformation, Equation 2 will be used. For the calculations, h_o was taken as 0.25 mm (this is the nominal maximum needle lift) and K_{def_needle} as $8 \cdot 10^{-13}$ m/Pa. The last parameter was calculated taking into account the realistic geometry of the needle, considering it as being a combination of several steel bars, with the methodology presented in [16]. Under these assumptions, from Equation 2, it can be seen that the maximum needle lift is 330 μ m at 100 MPa of P_{rail} , which represents an increase of 32% of the nominal maximum needle lift. Similar results are reported in [16]. It can be concluded that the needle deformation can be very important in diesel injectors because of the high pressure levels.

3.2 Effect of the needle deformation on pressure losses at the needle seat

Before giving details of the second step, the nomenclature that will be used to perform the analysis of the needle deformation on the pressure losses is shown in Figure 3. The injector is divided in three main parts: the injector holder (subscript “IH”), the needle

seat (subscript “seat”) and the orifice (subscript “orif”). Each part is characterised by its discharge coefficient (C_d), its cross-sectional area (A), and its pressure loss (ΔP).

The effect of the needle deformation on the pressure losses will be analysed through the following equation:

$$\Delta P_{IH+seat_with_deformation} = \Delta P_{IH} + \Delta P_{seat} \quad (3)$$

where ΔP_{IH} are the pressure losses in the injector holder, which will be obtained by the Darcy-Weisbach equation [23], and ΔP_{seat} are the pressure losses at the cross-sectional area defined by the needle surface and the needle seat, which will be obtained from Equation 4, showing the flow through the needle seat:

$$\dot{m}_f = \sqrt{2 \cdot \Delta P_{seat_with_deformation} \cdot \rho_f} \cdot (C_d \cdot A(h))_{seat} \quad (4)$$

In this Equation $(C_d \cdot A(h))_{seat}$ is equal to $C_{d_seat} \cdot A_{seat}(h)$, where A_{seat} is the cross-sectional area at the needle seat, and C_{d_seat} the corresponding discharge coefficient. To solve Equation 3, the pressure losses at the injector holder need to be determined first. For this purpose, as mentioned before, the Darcy-Weisbach equation will be used considering the internal geometry of the injector holder as a pipe. It was found that these pressure losses are very small, and they can be neglected. The detailed analysis of these pressure losses is presented in Appendix 1. Taking into account this fact, Equation 3 is simplified as follows:

$$\Delta P_{IH+seat_with_deformation} = \cancel{\Delta P_{IH}} + \Delta P_{seat} = \Delta P_{seat} \quad (5)$$

where ΔP_{seat} will be found from Equation 4 that was shown previously. But to use this equation both A_{seat} and C_{d_seat} need to be known. The details about how to determine these two parameters are shown in Appendix 2 and 3, respectively, and only a brief summary will be given in the following paragraphs.

A_{seat} will be found from Equation 15, which is defined in Appendix 2. This equation takes into account the detailed geometry of the seat and the needle, as well as the needle lift.

$C_{d_{seat}}$ will be obtained from the information presented in Figure 2. It is assumed that this parameter (which is a function of the Reynolds number) is the same with or without needle deformation. This means that the C_d of the needle seat is assumed to be a given function of Re at any *maximum* needle lift, i.e. at any value of the maximum cross-sectional area. It is worthy to underline that this is an acceptable choice taking into account that the needle is always at its highest position (maximum lift) in the present calculations. The details on how $C_{d_{seat}}$ was obtained are presented in Appendix 3.

3.3 Relationship between mass flow rate and pressure drop in the nozzle

Finally, to complete the analysis, the nozzle will be studied now. Depending on the number of orifices and their diameter, the relationship between the mass flow rate and the pressure drop across the orifices will be different. This relationship can be established taking into account the nozzle permeability, which will allow to obtain the value of $(C_d \cdot A)_{orif}$. The nozzle permeability is a standard parameter that is commonly used by nozzle manufacturers to quantify the flow through a nozzle. It is obtained by measuring the volume of fuel injected by the nozzle at a P_{rail} of 10 MPa and a P_{back} of 0.1 MPa during 30 seconds³. Its units are *cc/30sec*. This parameter can be related to the mass flow rate with the following equation:

$$\rho_f [kg/m^3] \cdot Permeability [cc/30sec] = \dot{m}_f [kg/s] \cdot \Delta t [sec] \quad (6)$$

If the different terms in Equation 6 are evaluated, the following equation is obtained:

³It is important to notice that the needle is removed in this kind of tests, and consequently only the flow through the nozzle orifices is characterised.

$$830 [kg/m^3] \cdot x [cc/30sec] = (C_d \cdot A)_{orif} \cdot \sqrt{2 \cdot 830 \cdot 9.9 \cdot 10^6} \cdot 30 [sec] \cdot 10^6 \quad (7)$$

where x is the permeability in $cc/30sec$. The term $(C_d \cdot A)_{orif}$ in Equation 7 can be isolated, giving the following expression:

$$(C_d \cdot A)_{orif} = \frac{830 \cdot x}{\sqrt{2 \cdot 830 \cdot 9.9 \cdot 10^6} \cdot 30 \cdot 10^6} \quad (8)$$

Finally, with this parameter, the relationship between \dot{m}_f and ΔP_{orif} ($=P_{sac} - P_{back}$) can be established:

$$\dot{m}_f = \sqrt{2 \cdot \Delta P_{orif} \cdot \rho_f} \cdot (C_d \cdot A)_{orif} \quad (9)$$

As a first approach, the value of $(C_d \cdot A)_{orif}$ will be assumed to be constant. Despite of this simplification the results will be qualitatively correct, as demonstrated later when considering a second approach. In this second approach, presented in the last section of this paper, data of a real nozzle will be used, where the discharge coefficient varies with Re .

3.4 Pressures losses calculation algorithm

To evaluate the pressure losses at any other operating condition (i.e. at any P_{rail} and P_{back}), the algorithm shown in Figure 4 will be used. This algorithm is explained in the following lines. The input data are P_{rail} , P_{back} and $(C_d \cdot A)_{orif}$. From this information the needle deformation is calculated (from Equation 2), and the cross-sectional area at the needle seat is determined (from Equation 15). Afterwards, P_{sac} is initially assumed to be equal to P_{rail} , and with this parameter the mass flow rate is calculated (with Equation 9). From this value and the cross-sectional area of the needle seat, C_{d_seat} is obtained (from Figure 10), and from all these parameters $\Delta P_{seat_with_deformation}$ (i.e., the pressure losses at the seat with needle deformation) is found (through Equation 4). From these pressure

losses, a new value of P_{sac} is found ($P_{sac_new} = P_{rail} - \Delta P_{seat_with_deformation}$). This new value is compared with the old one, and if they are equal the calculation is ended. Otherwise, the calculation is repeated with the new value until convergence is reached.

The previous algorithm (shown in Figure 4) was applied to several virtual nozzles with permeabilities between 60 and 680 $cc/30sec$, considering a back pressure of 5 MPa. The results are shown in Figure 5 in a surface P_{sac}/P_{rail} vs. P_{rail} (the ratio P_{sac}/P_{rail} is an indicator of the pressure losses at the injector) where different permeability curves are plotted. The three points connected by a fitted curve appearing in the Figure correspond to three different operating points of a real nozzle, which will be described and discussed in section 4. It is surprising that, for a given permeability, the pressure losses increase with the rail pressure, first, and they decrease afterwards. This change in the trend of the curve is caused by the needle deformation, as demonstrated in Figure 6, where the needle deformation effect was removed. From this new Figure, it is evident that the trend of the different permeability curves is monotonic (the pressure losses increase with the rail pressure). The comparison between Figures 5 and 6 shows, on the one hand, that the effect of the needle deformation is not negligible, and consequently it is important to take it into account for pressure losses characterisation. On the other hand, it can be observed that the needle deformation reduces the value of the pressure losses, but even though they still have a significantly high value.

Another important observation from Figure 5 is that pressure losses are not far from being proportional to P_{rail} , because the different curves tend to be horizontal lines⁴. This result indicates that pressure losses in the injector ($P_{rail} - P_{sac}$) are more or less proportional to the pressure drop in the nozzle orifice ($P_{sac} - P_{back}$), even if the pressure losses are not negligible. Consequently, concerning the two implicit hypotheses mentioned in the introduction of this paper when talking about the common assumption of considering $P_{sac} = P_{rail}$ when studying the flow in the nozzle, the first one (that the pressure losses along

⁴A horizontal line in this plot means that the ratio P_{sac}/P_{rail} is constant. Therefore P_{sac} is proportional to P_{rail} and, consequently, $P_{rail} - P_{sac}$ is also proportional to P_{rail} .

the injector are small compared to the rail pressure) is false whereas the second one (that the pressure losses are proportional to the pressure drop at the nozzle orifice) seems to be approximately correct. Because of this, it is possible to neglect pressure losses in the injector when the results of internal flow are being compared qualitatively, but it is an error to neglect these pressure losses if these data are used quantitatively (for instance when modelling results are compared to experimental results).

P_{rail} affects both the mass flow rate and the needle deformation. The effect of this parameter on needle deformation is straightforward (as analysed at the beginning of this section), whereas its effect on the mass flow rate is not direct, because also the nozzle permeability does play an important role. In order to analyse the effect of nozzle permeability on the pressure losses, three different nozzles were selected (with permeabilities of 60, 340 and 680 $cc/30sec$) in Figure 5, all of them plotted with a thicker line. For the low permeability nozzle (60 $cc/30sec$), which corresponds to a single-hole nozzle, it can be observed that the pressure losses are really small (around 1% of P_{rail}), whereas for the two other nozzles with higher permeability (340 and 680 $cc/30sec$), which correspond to multi-hole nozzles, pressure losses can be very significant. Therefore, the comparison of results of internal flow between single-hole and multi-hole nozzles should be performed carefully.

It is important to underline that the nozzles analysed up to now correspond to virtual nozzles with a constant $(C_d \cdot A)_{orif}$. In the next section the pressure losses in a real nozzle (where $(C_d \cdot A)_{orif}$ varies with the operating conditions) will be analysed.

4 Analysis of the pressure losses in an injector with a real nozzle

The real nozzle to analyse corresponds to a multi-hole nozzle, with conical orifices (k-factor 1.7) of an outlet diameter of 138 μm , and a permeability of 343 $cc/30sec$ (in

the standard conditions employed by Bosch: P_{rail} 10 MPa and P_{back} 0.1 MPa). The mass flow rate was measured experimentally at three different operating conditions. The main details of the experiments are shown in Table 1. It is worthy to mention that the C_{d_global} shown in this Table corresponds to the discharge coefficient of the whole injector (injector holder plus nozzle), which is obtained by solving the following equation:

$$\dot{m}_f = \sqrt{2 \cdot (P_{rail} - P_{back}) \cdot \rho_f \cdot C_{d_global} \cdot A_{orif}} \quad (10)$$

The calculation of the pressure losses for the three conditions presented in Table 1 was performed using all the concepts and equations already presented in Section 3 (i.e. taking into account the needle deformation). However, as now C_{d_global} , P_{rail} and P_{back} are known, the algorithm shown in Figure 4 can not be used anymore. A new algorithm to perform this calculation will be explained in the following lines. The input data are P_{rail} , P_{back} , C_{d_global} , and \dot{m}_f . From this information the needle deformation, h , is calculated (from Equation 2), and the cross-sectional area at the needle seat, A_{seat} , is determined (from Equation 15). With this parameter and the mass flow rate, C_{d_seat} is found (with Figure 10), and with all these parameters $\Delta P_{seat_with_deformation}$ (i.e. the pressure losses at the needle seat with needle deformation) is obtained (from Equation 4). Finally, P_{sac} can be obtained (equal to $P_{rail} - \Delta P_{seat_with_deformation}$). The results obtained are shown in Figure 7. These three cases are also plotted in Figure 5 keeping the same symbols. It can be observed that, on the one hand, the trend when using a real nozzle is the same as it was obtained previously for virtual nozzles (P_{sac}/P_{rail} decreases first and increases afterwards as P_{rail} increases), and thus the information shown in Figure 5 is qualitatively correct. Consequently, to assume that $(C_d \cdot A)_{orif}$ is constant for the virtual nozzles was a sensible choice. On the other hand, it can also be observed that there is a mismatch between the permeability value for the real nozzle and those for the virtual ones (the nozzle permeability is 343 cc/30sec, but the three points fall between the curves of 360 and 400 cc/30sec). This fact simply demonstrates that the nozzle permeability is a parameter that is unable to appropriately represent the nozzle behaviour at real engine operating

conditions. But this topic is well beyond the scope of this paper.

Finally, let's assume that case 3 in Table 1 is intended to be modelled with CFD. If P_{sac} is assumed to be the same as P_{rail} , to neglect pressure losses leads to an error of 15% in pressure, according to Figure 7. This error is not small, and therefore it is convenient to be careful when modelling the flow through the nozzle if it is later compared to experimental data.

5 Conclusions

A methodology to determine pressure losses in a common rail diesel injector was defined. This methodology combines experimental data and theoretical calculations based on the physics of the phenomena involved. Using this methodology, the following conclusions were extracted:

- Needle deformation can be very significant. In the injector studied here, the maximum needle lift increases from 250 μm to 330 μm (so 32% higher) at $P_{rail} = 100$ MPa.
- Needle deformation affects pressure losses. The trend is that an increase in needle deformation reduces pressure losses.
- Even if the needle deformation is taken into account, pressure losses can be important. For the injector used in this work, they can be around 15% of the rail pressure for a medium permeability nozzle (340 $cc/30sec$) and around 30% of the rail pressure for a high permeability nozzle (680 $cc/30sec$).

It is worthy to underline that special attention should be paid, on the one hand, when results relative to the injection (internal flow, spray atomization, spray penetration..) and combustion processes from single-hole nozzles (i.e. low permeability nozzles) are intended to be extrapolated to multi-hole nozzles (i.e. nozzles with much higher permeability),

because pressure losses can be important in the latter case whereas they aren't in the first case, and, on the other hand, if these results in nozzles coming from modelling are compared with those coming from experiments, because P_{sac} and P_{rail} can be significantly different from each other. As an additional remark, people working on the study of the injection and/or combustion processes, both experimentally or through simulations, will find in this work some interesting information to better know the actual injection pressure to be used in their analysis and/or simulations.

Acknowledgements

The authors would like to thank José Enrique del Rey and Daniel Lérica, both members of CMT-Motores Térmicos of the Universitat Politècnica de València, for their help with the experimental work. They also thank the FPU program of the Ministerio de Educación of Spain for granting the PhD. studies of Oscar A. de la Garza.

References

1. Walsh, M., 2001. "Global trends in diesel emissions regulations - a 2001 update". *SAE Paper 2001-01-0183*.
2. Johnson, T., 2009. "Review of diesel emissions and control". *Int. J. Engine Res.*, **10**(5), pp. 275–285.
3. Deng, J., Bastian, M., and Stobart, R., 2012. "Particulate matter prediction in both steady state and transient operation of diesel engines". *Proceedings of the Institution of Mechanical Engineers, Part D: Journal of Automobile Engineering*, **226**(2), pp. 260–274.
4. Kent, J., and Brown, G., 1983. "Nozzle exit flow characteristics for square-edged and rounded inlet geometries". *Combustion Science and Technology*, **30**, pp. 121–132.

5. Karasawa, T., Tanaka, M., Abe, K., and Shiga, S., 1992. “Effect of nozzle configuration on the atomization of a steady spray”. *Atomization and Sprays*, **2**, pp. 411–426.
6. Koo, J., Hong, S., Shakal, J., and Goto, S., 1997. “Influence of fuel injector nozzle geometry on internal and external flow characteristics”. *SAE Paper 970354*.
7. Payri, R., Molina, S., Salvador, F., and Gimeno, J., 2004. “A study of the relation between nozzle geometry, internal flow and spray characteristics in diesel fuel injection system”. *KSME International Journal*, **18**(7), pp. 1222–1235.
8. Desantes, J., Payri, R., Pastor, J., and Gimeno, J., 2005. “Experimental characterization of internal nozzle flow and diesel spray behavior. part i: nonevaporative conditions”. *Atomization and Sprays*, **15**, pp. 489–516.
9. Benajes, J., Molina, S., González, C., and Donde, R., 2008. “The role of nozzle convergence in diesel combustion”. *Fuel*, **87**, pp. 1849–1858.
10. Nishida, K., Gao, J., Manabe, T., and Zhang, Y., 2008. “Spray and mixture properties of evaporating fuel spray injected by hole-type direct injection diesel injector”. *Int. J. Engine Res.*, **9**(4), pp. 347–360.
11. Gavaises, M., 2008. “Flow in valve covered orifice nozzles with cylindrical and tapered holes and link to cavitation erosion and engine exhaust emissions”. *Int. J. Engine Res.*, **9**(6), pp. 435–447.
12. Jung, D., and Assanis, D., 2008. “A reduced quasi-dimensional model to predict the effect of nozzle geometry on diesel engine performance and emissions”. *Proceedings of the Institution of Mechanical Engineers, Part D: Journal of Automobile Engineering*, **222**(1), pp. 131–141.
13. Payri, R., Salvador, F., Gimeno, J., and de la Morena, J., 2009. “Effects of nozzle geometry on direct injection diesel engine combustion process”. *Applied Thermal Engineering*, **29**, pp. 2051–2060.

14. Fimml, W., Chmeta, F., Pirker, G., and Wimmer, A., 2010. “Influence of cavitation in the injection nozzle on combustion in diesel engines”. *Int. J. Engine Res.*, **11**(5), pp. 375–390.
15. Desantes, J., Arrègle, J., López, J., and Hermens, S., 2005. “Experimental characterization of outlet flow for different diesel nozzle geometries”. *SAE Paper 2005-01-2120*.
16. Desantes, J., Arrègle, J., and Rodríguez, P., 1999. “Computational model for simulation of diesel injection system”. *SAE Paper 1999-01-0915*.
17. Arcoumanis, C., and Gavaises, M., 1999. “Modeling of advanced high-pressure fuel injection systems for passenger car diesel engines”. *SAE Paper 1999-01-0910*.
18. Yamanishi, M., 2004. “Application of a computer model to various specifications of fuel injection systems for diesel engines”. *JSME International Journal Series B*, **46**(2), pp. 326–331.
19. Becchi, G., 1971. “Analytical simulation of fuel injection in diesel engines”. *SAE Paper 710568*.
20. Lee, J., Cho, S., Lee, S., and Bea, C., 2002. “Bouncing of the diesel injector needle at the closing stage”. *Proc. Instn. Mech. Engrs. Part D: J. Automobile Engineering*, **216**(8), pp. 691–700.
21. Smith, W., and Timoney, D., 1992. “Fuel injection rate analysis - a new diagnostic tool for combustion research”. *SAE Paper 922224*.
22. Dongiovanni, C., and Coppo, M., 2010. “Accurate modelling of an injector for common rail systems”. In *Fuel injection*, D. Siano, ed. Sciyo, ch. 6.
23. Nakayama, Y., and Boucher, R., 1999. *Introduction to fluid mechanics*. Butterworth/Heinemann.
24. Imagine, 2010. *Lab AMESim v.8, User’s Manual*. LMS Imagine.

Appendix 1. Injector holder pressure losses calculation

The mass flow rate through the injector holder can be written in the following way:

$$\dot{m}_f = \sqrt{2 \cdot \Delta P_{IH} \cdot \rho_f} \cdot (C_d \cdot A)_{IH} \quad (11)$$

The injector holder internal geometry can be considered as a pipe, and therefore the pressure losses can be determined by the Darcy-Weisback equation [23]:

$$\Delta P_{IH} = \frac{f \cdot \rho_f \cdot u^2 \cdot L}{2 \cdot D} \quad (12)$$

where ΔP_{IH} are the pressure losses in the injector holder in Pa, f is the friction coefficient (which is non-dimensional), ρ_f is the fuel density (830 kg/m^3 for a standard diesel fuel), u is the fluid velocity in m/s , L is the length of the internal pipe of the injector holder (0.115 m in the present case), and D is the diameter of this internal pipe (0.00216 m for the injector holder considered here).

Concerning the friction coefficient, it will be obtained as follows:

- For laminar flows ($Re < 2000$), the equation of Poiseuille [23] will be used:

$$f = \frac{64}{Re} \quad (13)$$

- For turbulent flows ($Re > 2000$), the equation of Swamee and Jain [23] will be employed:

$$f = \frac{0.25}{\left[\log \left(\frac{\varepsilon}{3.71 \cdot D} + \frac{5.74}{Re^{0.9}} \right) \right]^2} \quad (14)$$

where ε is the roughness of the surface.

With all these equations ΔP_{IH} was calculated for \dot{m}_f ranging from 0.5 to 50 g/s . The results are shown in Figure 8, which demonstrate that these pressure losses at the injector

holder are very small, and can be neglected. In these calculations ε was considered as being 0.1 mm , a value that is surely much higher than the actual one taking into account the good surface finish typical in diesel nozzles. But even with this pessimistic choice the pressure losses are negligible. Consequently, it can be concluded that the pressure losses in the injector holder can be neglected.

Appendix 2. Cross-sectional area between the needle and the needle seat

The area between the needle surface and the needle seat was calculated with Equation 15, taken from the AMESim[®] User Manual [24]:

$$A(h)_{seat} = \left(D_S - h \cdot \sin \frac{\alpha}{2} \cdot \left[\cos \frac{\alpha}{2} + \sin \frac{\alpha}{2} \cdot \tan \beta_1 \right] \right) \cdot \frac{\pi \cdot h \cdot \sin \frac{\alpha}{2}}{\cos \beta_1} \quad (15)$$

In Figure 9 the main parameters of Equation 15 are shown. D_S is the sac diameter, the value of which is 0.57 mm . h is the needle lift, its value being known from Equation 2. $\frac{\alpha}{2}$ is the half-angle of the needle tip, which is 30° . The value of $\tan \beta_1$ is defined as follows:

$$\tan \beta_1 = M_1 - \sqrt{M_1^2 - 0.5} \quad (16)$$

where M_1 is defined as follows:

$$M_1 = 0.25 \cdot \left(\frac{D_S \cdot \sin \frac{\alpha}{2}}{h \cdot \left(\sin \frac{\alpha}{2} + M_2 \right)} \cdot \left[1 + \frac{1}{\tan^2 \frac{\alpha}{2}} \right] - \frac{1}{\tan \frac{\alpha}{2}} \right) \quad (17)$$

and M_2 is:

$$M_2 = \frac{(D_A - D_S) \cdot \cos \frac{\alpha}{2}}{2 \cdot \tan \frac{\sigma}{2}} \cdot \left(\tan \frac{\alpha}{2} - \tan \frac{\sigma}{2} \right) \quad (18)$$

where D_A is the diameter of the needle where its cone angle changes (its value is 0.616 mm in the studied case) and $\frac{\sigma}{2}$ is the half-angle of the needle seat, which is 30° .

Appendix 3. C_{d_seat} calculation

The value of C_{d_seat} will be obtained from the information in Figure 2. More precisely, the following steps and hypotheses will be taken:

- ΔP_{IH} will be neglected (as justified in Appendix 1).
- Because of the previous assumption, the information of Figure 2 corresponds to ΔP_{seat}
- A_{seat} will be found using Equation 15. For this calculation the actual needle lift, h , will be calculated considering the actual value of P_{rail} at each operating point.
- To determine C_{d_seat} in the range of mass flow rates covered by the fit shown in Figure 2, Equation 4 will be used.

The obtained results are shown in Figure 10, where C_{d_seat} is plotted as a function of Re , which is defined as follows:

$$Re = \frac{u \cdot d_{h_seat} \cdot \rho_f}{\mu} \quad (19)$$

where u is the mean velocity, which can be deduced from the continuity equation ($\dot{m}_f = u \cdot \rho_f \cdot A_{seat}$), d_{h_seat} is the hydraulic diameter of the needle, defined as $\sqrt{\frac{4 \cdot A_{seat}}{\pi}}$, ρ_f is the fuel density (830 kg/m^3), and μ is the fuel dynamic viscosity, the value of which is $0.00367 \text{ kg/(m} \cdot \text{s)}$.

It is worthy to underline that the relationship between C_{d_seat} and Re found here comes from the experimental data shown in Figure 2, which is strictly only valid for the type of injector holder used in the present experiment. However, as already mentioned in the text, this one is representative of those currently used in automotive applications, and consequently the results of the present paper can also be taken as representative of what might be expected in other injectors similar to the one investigated here.

List of Figures

1	Schematics of the experimental facility to measure the injector pressure losses.	23
2	Pressure losses in the injector.	24
3	Schematics of a common rail diesel injector showing the notation used in the study.	25
4	Algorithm to calculate pressure losses at any other operating condition (P_{rail} and P_{back}).	26
5	Evolution of P_{sac}/P_{rail} as a function of P_{rail} for several virtual nozzles with permeabilites between 60 to 680 $cc/30sec$. The three points connected by a fitted curve correspond to three different operating points of a real nozzle, which will be described and discussed in section 4.	27
6	Evolution of P_{sac}/P_{rail} as a function of P_{rail} for several virtual nozzles with permeabilites between 60 to 680 $cc/30sec$. In contrast with Figure 5, the needle deformation is now not taken into account for the calculations.	28
7	Pressure losses for the three operating conditions shown in Table 1 corresponding to a real nozzle.	29
8	Pressure losses in the injector holder.	30
9	Effective area between the needle surface and its seat.	31
10	$C_{d_{seat}}$ as a function of Re	32

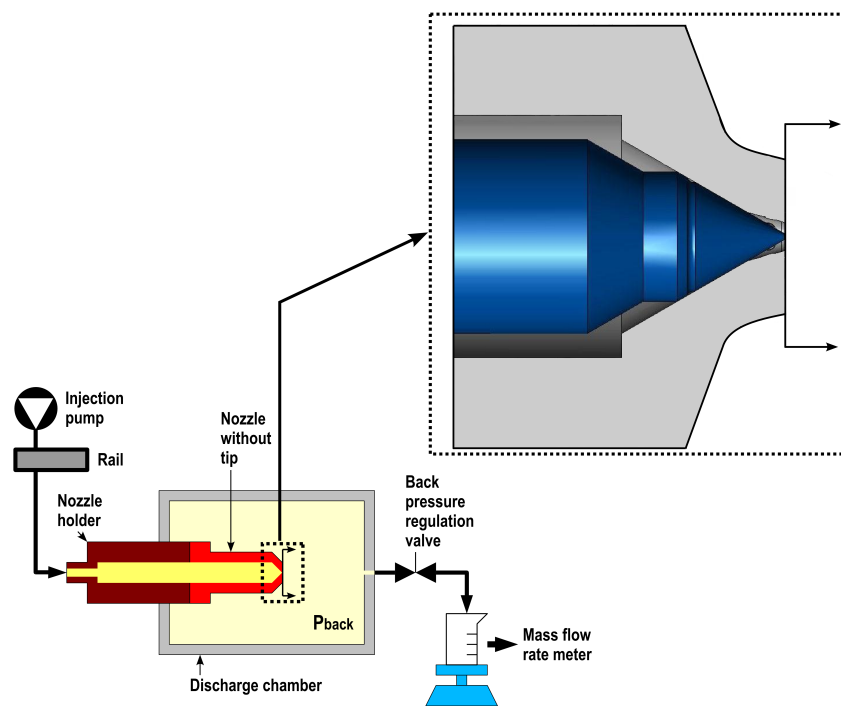


Figure 1: Schematics of the experimental facility to measure the injector pressure losses.

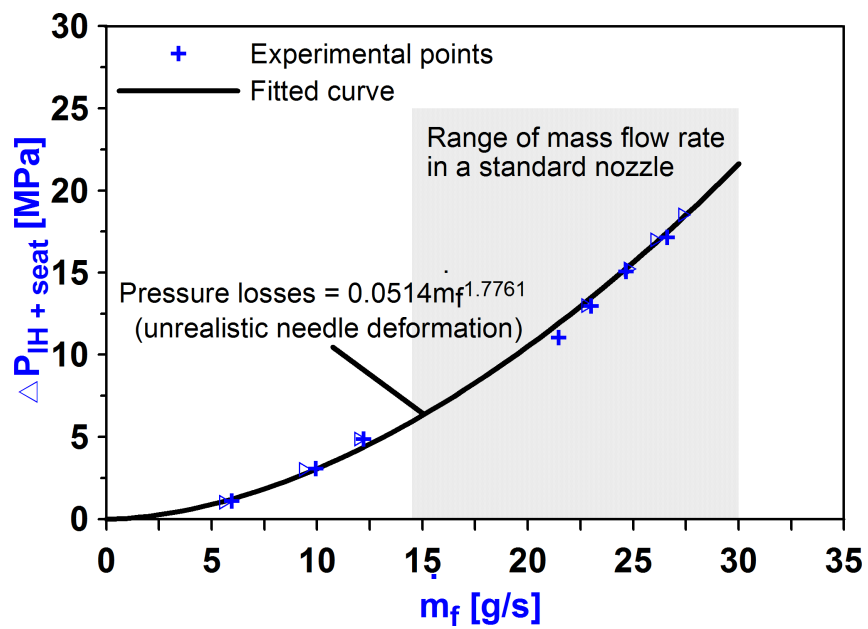


Figure 2: Pressure losses in the injector.

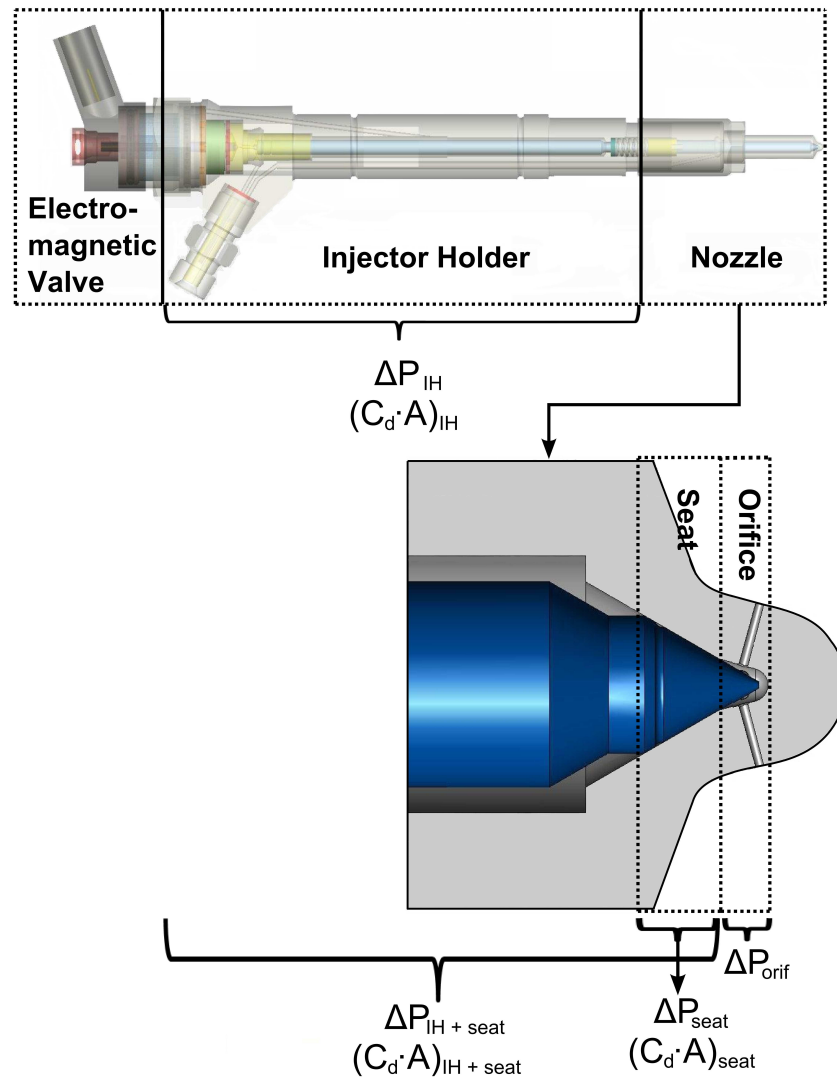


Figure 3: Schematics of a common rail diesel injector showing the notation used in the study.

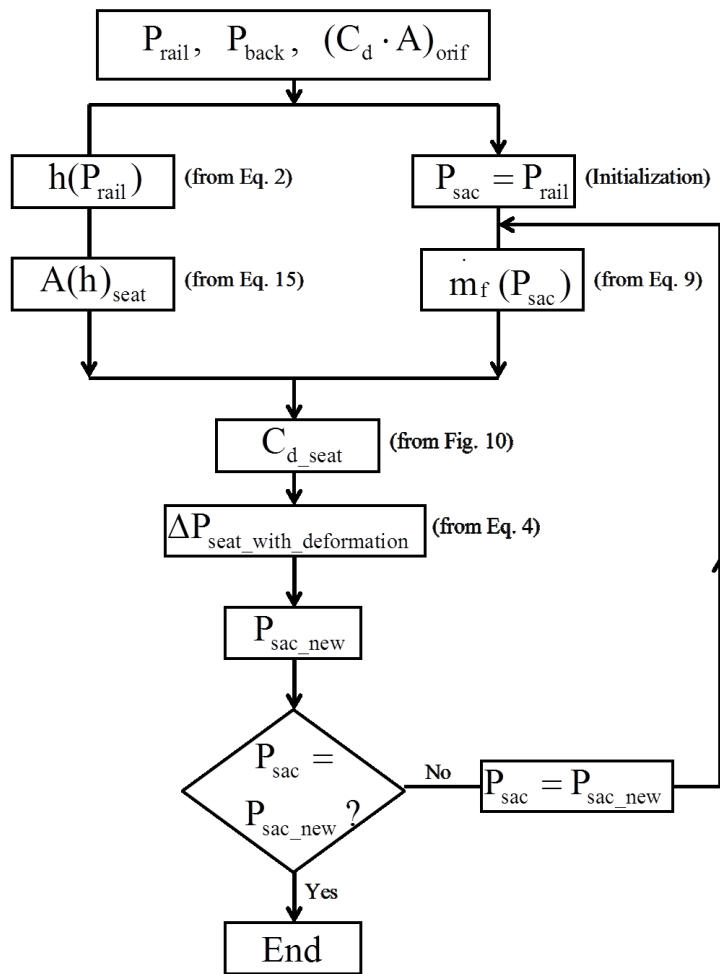


Figure 4: Algorithm to calculate pressure losses at any other operating condition (P_{rail} and P_{back}).

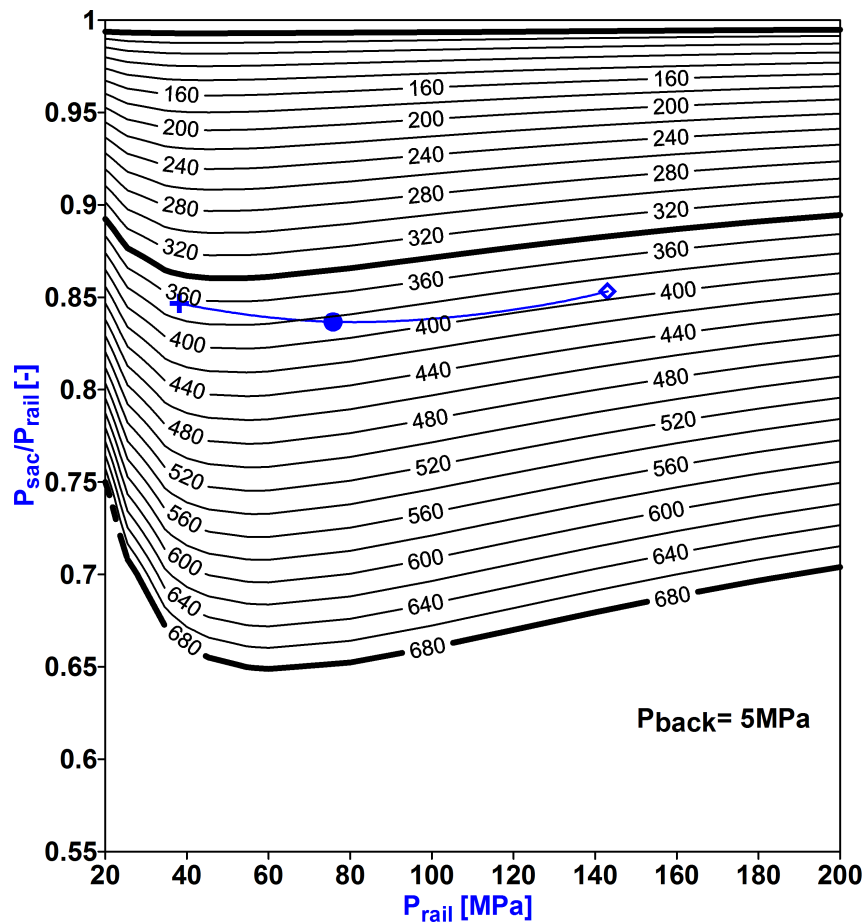


Figure 5: Evolution of P_{sac}/P_{rail} as a function of P_{rail} for several virtual nozzles with permeabilities between 60 to 680 $cc/30sec$. The three points connected by a fitted curve correspond to three different operating points of a real nozzle, which will be described and discussed in section 4.

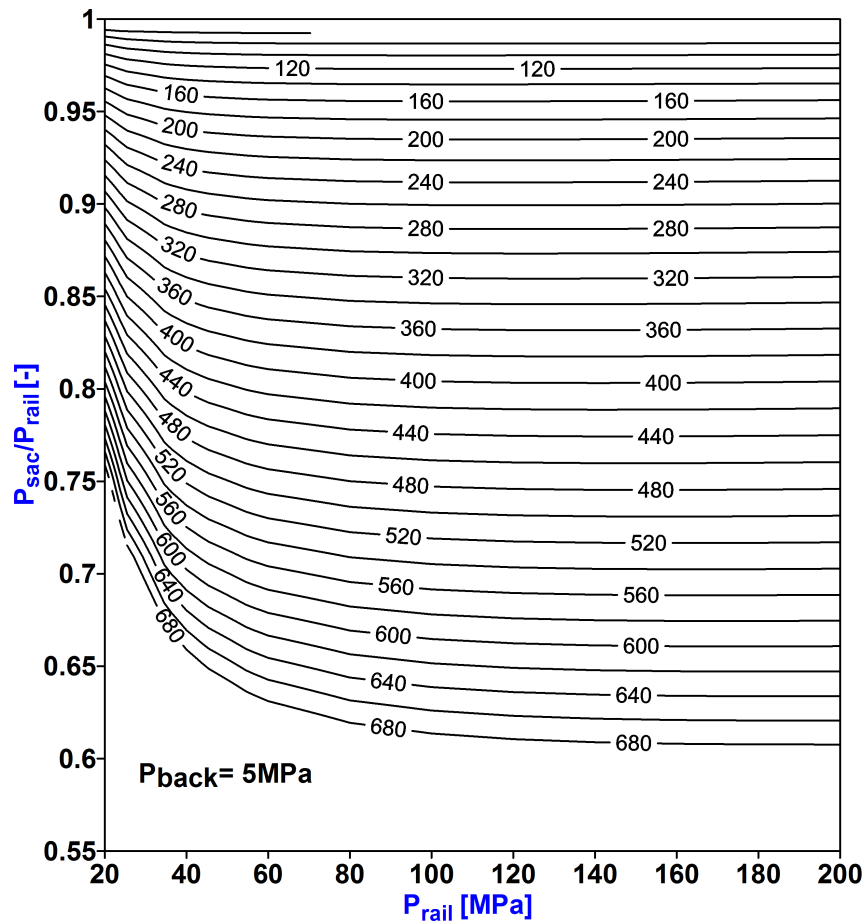


Figure 6: Evolution of P_{sac}/P_{rail} as a function of P_{rail} for several virtual nozzles with permeabilities between 60 to 680 $cc/30sec$. In contrast with Figure 5, the needle deformation is now not taken into account for the calculations.

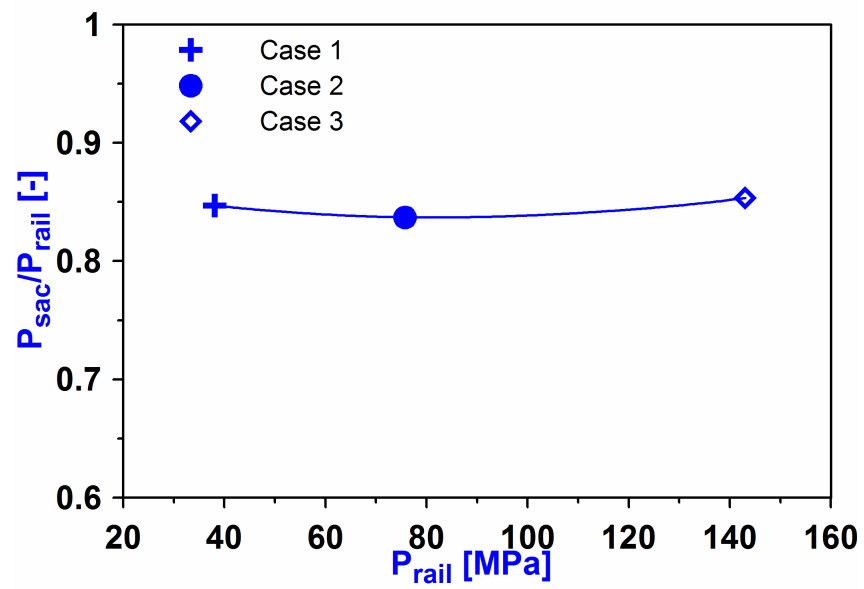


Figure 7: Pressure losses for the three operating conditions shown in Table 1 corresponding to a real nozzle.

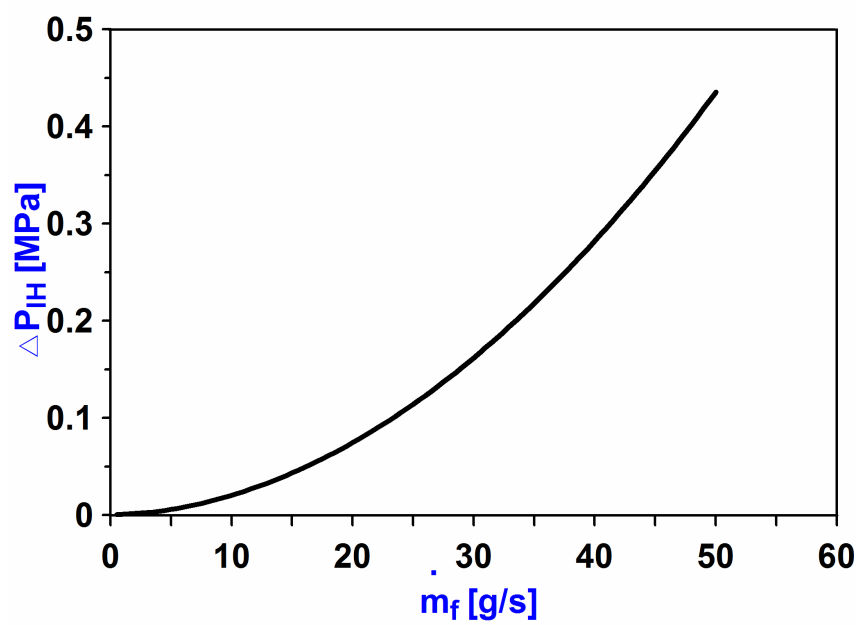


Figure 8: Pressure losses in the injector holder.

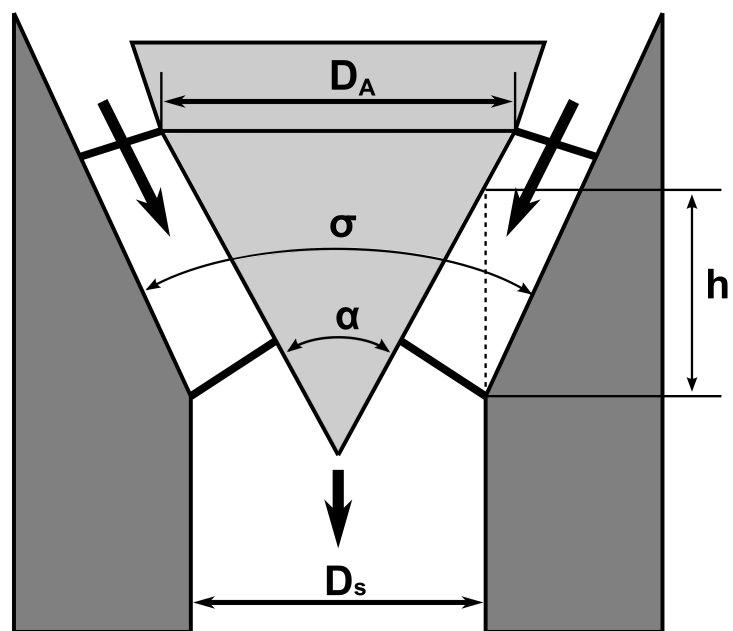


Figure 9: Effective area between the needle surface and its seat.

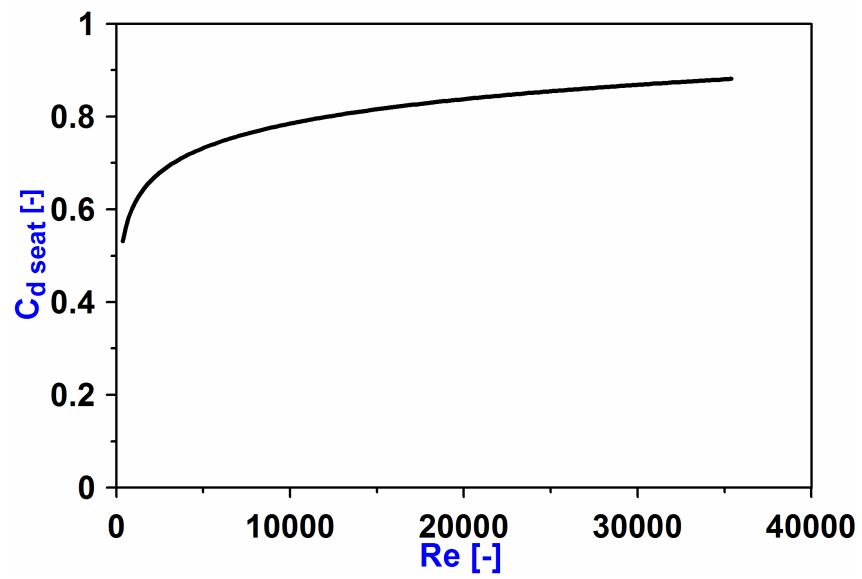


Figure 10: $C_{d,seat}$ as a function of Re .

List of Tables

- 1 Operating conditions and results of the three different experimental cases. . 34

Case	P_{rail}	P_{back}	C_{d_global}	\dot{m}_f
	[MPa]	[MPa]	[-]	[kg/s]
1	38.06	10.02	0.78	0.015
2	75.73	10.06	0.82	0.024
3	143.02	9.92	0.84	0.036

Table 1: Operating conditions and results of the three different experimental cases.